

## Traveling Waves and Defect-Initiated Turbulence in Electroconvecting Nematics

Ingo Rehberg,<sup>(a)</sup> Steffen Rasenat,<sup>(a)</sup> and Victor Steinberg

*Department of Nuclear Physics, Weizmann Institut, 76100 Rehovot, Israel*

(Received 31 May 1988; revised manuscript received 12 September 1988)

A novel time-dependent state in the form of traveling waves in electrohydrodynamic convection in a thin ( $15\ \mu\text{m}$ ) cell of very large aspect ratio is experimentally studied. The transition leading to uniform waves is a continuous one bifurcating directly from the homogeneous state. The onset of spatiotemporal turbulence in this 2D system is characterized by the appearance of topological defects. The number of defects increases with the control parameter, and their statistical distribution is in very good quantitative agreement with a theoretical curve recently derived for "topological turbulence."

PACS numbers: 47.25.Ae, 47.65.+a

Considerable experimental and theoretical efforts have been made during recent years to describe and understand spatiotemporal chaotic behavior by deriving tractable models, and performing experiments with systems that can be described by these models. From these studies the most promising and experimentally attractive system appears to be one which shows transition to spatiotemporal turbulence from an oscillatory state. It was suggested recently that a system exhibiting a transition to an oscillatory instability as a first bifurcation, namely convection in a binary mixture,<sup>1</sup> is a good candidate to study spatiotemporal complex behavior quantitatively. This system can be described by a generalized Ginzburg-Landau (GGL) equation with complex coefficients derivable from basic hydrodynamic equations. The theoretical and numerical studies of the GGL equation show that spatiotemporal complex behavior occurs as a result of modulational, or Benjamin-Feir, instability of the wave pattern,<sup>2</sup> and may have a universal route to spatiotemporal turbulence. Recently the direct transition from conduction to spatiotemporal chaotic states was indeed observed in convective binary mixtures.<sup>3</sup> Because of the degeneracy of the wave vector in the horizontal plane, the pattern behavior is pretty elaborate, containing different types of defects, and surely cannot be described by a low-dimensional attractor. In spite of the fact that a qualitatively similar pattern dynamics was recently reproduced by numerical simulations of the GGL equation,<sup>4</sup> the main problem remains how to characterize 2D spatiotemporal pattern behavior of traveling waves (TW) in order to compare it with theoretical and numerical results.

In this Letter we report about another system which shows a continuous transition from the spatially homogeneous state to a uniform TW pattern, namely electrohydrodynamic convection in a thin layer of a nematic liquid crystal. This system has three crucial advantages compared to convection in binary mixtures: (i) The transition to TW is a continuous one at a finite frequency and a finite wave number which makes the system very attractive for experimental studies of the linear and non-

linear properties of the oscillatory instability. (ii) Very large aspect ratio (up to 1000 rolls) and convenient range of frequencies make it a good candidate to study the transition to spatiotemporal turbulence in extended systems with propagative patterns. (iii) The direction of the wave vector of TW is fixed due to the sample preparation that erases the degeneracy of the wave vector in the horizontal plane making the system anisotropic. As a consequence of this the transition from uniform saturated TW to spatiotemporal, chaos occurs via a simple scenario of topological defect (dislocation) nucleation. Thus, this transition can be traced and studied quantitatively. Moreover, recently the role of the phase turbulence as a defect generator in 2D TW systems has been studied theoretically and numerically.<sup>5</sup> In the region of a weak Benjamin-Feir instability, a phase perturbation leads to the creation of topological defects.<sup>5</sup> This defect-initiated turbulent regime called "topological turbulence" was studied numerically for the GGL equation of an anisotropic flow and showed strikingly similar spatiotemporal pattern behavior to the experimental results presented here.<sup>5</sup>

The experimental setup is the standard one<sup>6</sup>: The nematic *N*-(*p*-methoxybenzylidene)-*p*-butylaniline (MBBA) is sandwiched between two transparent glass electrodes with a distance of  $15\ \mu\text{m}$  and lateral dimensions of the cell  $L_x = 2\ \text{cm}$  (perpendicular to the rolls) and  $L_y = 0.5\ \text{mm}$  (aspect ratio 1-33-1300). The cell temperature is regulated to  $25^\circ\text{C}$  with a stability of  $\pm 0.005\ \text{K}$  by circulating water flow. Together with proper sample handling and preparation, this turns to be a crucial factor to reach a reasonable short-term stability and reproducibility within several hours (see Fig. 3 below). However, sample aging during several weeks was still observed.

When applying an ac voltage to the cell, the molecular orientation described by the director is stable in the planar alignment along the  $x$  axis below a well defined threshold voltage. Above this frequency-dependent (see Fig. 4 below) threshold, electroconvection in the form of parallel rolls with the axis along the  $y$  direction and trav-

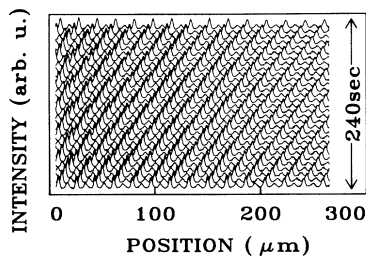


FIG. 1. Light intensities measured along a line perpendicular to the orientation of the rolls within time intervals of 8 s plotted on top of each other.

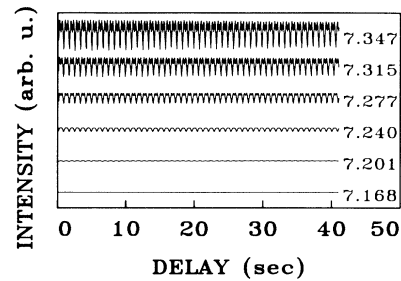


FIG. 2. The structure function measured at a fixed position for different driving voltages.

eling along the  $x$  direction sets in. Coupling between velocity and molecular orientation causes a spatially periodic intensity modulation of the light field behind the cell, and the modulation amplitude is proportional to the velocity of the flow.<sup>7</sup> The image of the pattern is observed with a video camera mounted on a polarizing microscope, digitized with a resolution of  $512 \times 512$  pixels of 256 grey levels and fed to a computer. Use of MBBA with cell heights larger than  $20 \mu\text{m}$  led to conventionally observed stationary convection patterns named Williams rolls. Decreasing the height below  $20 \mu\text{m}$  caused a bifurcation to traveling convection rolls (TW) as demonstrated in Fig. 1. It presents only a small part of TW in the cell. There is a hint for a theoretical explanation of this TW: For a thin cell the director and charge relaxation time become of the same order. The exact critical thickness is expected to be a function of the electrical conductivity of the sample. However, no exact calculation explaining TW is available at the moment.

Quantitative information about TW is obtained from the intensity structure function, which is the properly normalized correlation function.<sup>8</sup> This provides informa-

tion about the onset, the speed, and the amplitude of TW, and the onset of chaos. Intensity structure functions for different voltages are shown in Fig. 2. The value 7.168 V is below the onset of TW. At 7.201 V, a modulation shows up indicating the onset of convection. The amplitude of this modulation grows with increasing voltage. The lack of decay in the structure function for a delay of about fifty oscillation periods indicates a reasonable overall stability of the experiment.

The results for the amplitude and the intensity modulation and the frequency obtained by a spectral analysis of the structure function presented in Fig. 3 clearly demonstrates that the bifurcation is forward at a finite frequency from the ground state without visible hysteretic behavior (squares and circles indicate stepping the voltage up and down, respectively). The fit to the expected square-root law of the order parameter determines the critical voltage  $V_c$ . The neutral frequency value  $f_0$  is also obtained from Fig. 3.  $V_c$  and  $f_0$  as functions of the external frequency are presented in Fig. 4. There the solid diamonds indicate the threshold value for TW and the crosses indicate their neutral frequency. Above the cutoff frequency of about 450 Hz, the ground state becomes unstable with respect to a different convective pattern, dielectric rolls.

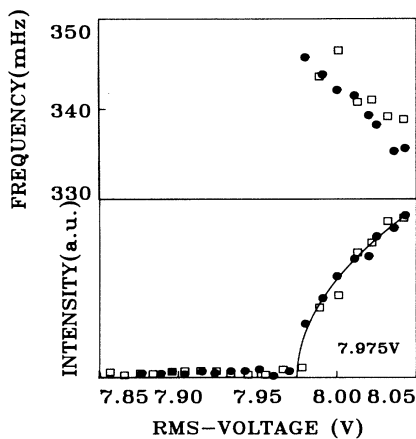


FIG. 3. The intensity modulation and the frequency obtained from structure functions measured at different voltages near the onset of TW. The solid line is a fit to the expected square-root law.

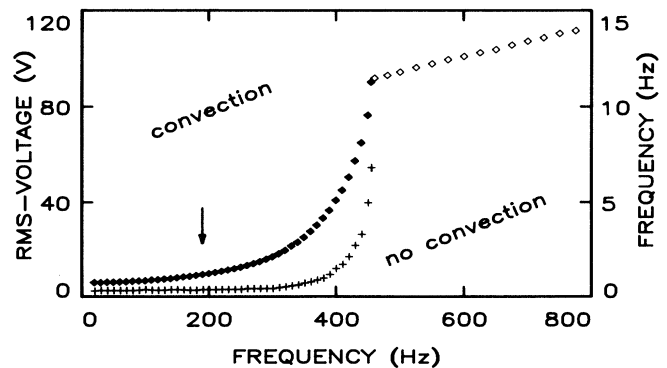


FIG. 4. Phase diagram. The ground state loses stability to TW (solid diamonds) or dielectric rolls (open diamonds). The crosses indicate the frequency of the TW at onset.

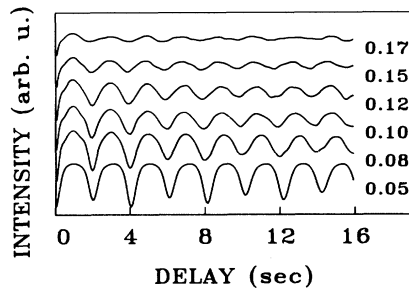


FIG. 5. The decay of the structure function for driving voltages above  $\epsilon=0.078$  indicates the onset of defect-mediated turbulence.

We would like to point out here that experimental results on localized TW in much thicker cells than used in our investigation were published very recently by Joets and Ribotta.<sup>9</sup> Their TW observed in a close vicinity of the cutoff frequency demonstrates very different qualitative and quantitative behavior. TW described in Ref. 10 never showed a uniform TW pattern near the threshold; its characteristic frequency is much higher and increases with the voltage opposite to the result shown in Fig. 3. Recent experimental and theoretical studies<sup>11</sup> show the occurrence of spatiotemporal modulated TW, caused by convectively unstable conditions. The transition from modulated to saturated TW occurs in close vicinity to the convection threshold. The question arises why in electroconvection we observed just saturated TW. A simple estimation showed that convectively unstable conditions in our case may be observed at  $\epsilon=V/V_c-1 < 0.001$ , which is closer to the onset than we studied.

We studied the onset of spatiotemporal chaos at a frequency of 190 Hz, i.e., pretty much in the middle of the TW regime. Here TW were stable up to  $\epsilon=0.078$ . The regularity of the motion ceases above this value as indicated by the decay of the structure functions shown in Fig. 5. This destruction of spatiotemporal order is stemming from the creation of pairs of topological defects. Increasing the voltage increases the nucleation rate of defects and their total number. Once created, the de-

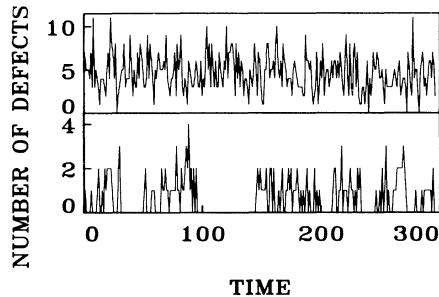


FIG. 7. Number of defects as a function of time for  $\epsilon=0.085$  (lower curve) and  $\epsilon=0.19$  (upper curve).

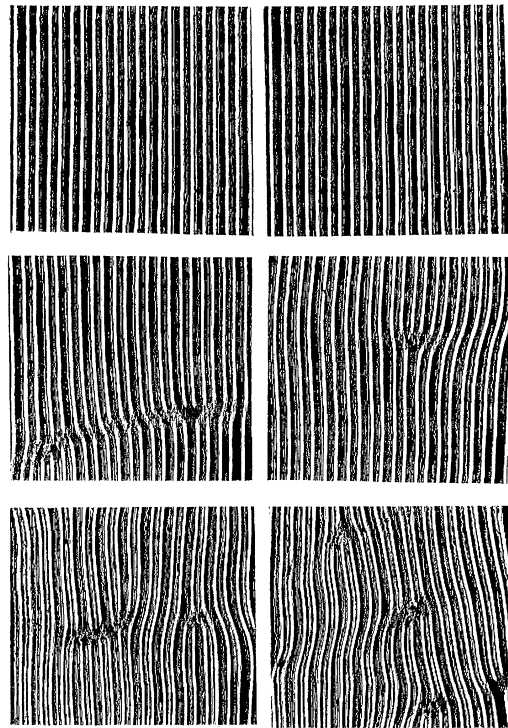


FIG. 6. Two images of the convection structure obtained at different times at  $\epsilon=0.05$  (upper two),  $\epsilon=0.10$  (middle two) and  $\epsilon=0.17$  (lower two).

fects move through the system before they annihilate in pairs. The disordered TW pattern is characterized by the presence and interaction of a large number of the moving dislocations. The scenario is illustrated in Fig. 6.

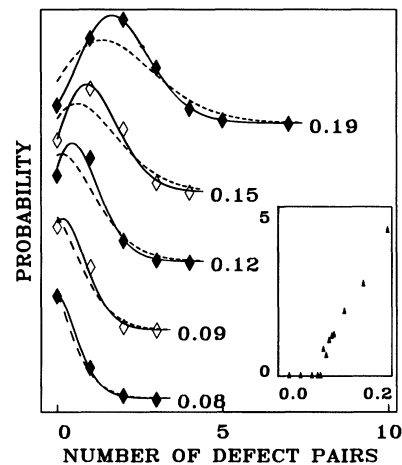


FIG. 8. Histogram of the defect statistic for different values of the driving voltages  $\epsilon$ . The solid lines are the corresponding squared Poisson distributions. The Poisson distributions (dashed lines) are shown for comparison. Inset: The mean number of defects as a function of  $\epsilon$ .

Three sets of pictures from a fixed square window containing about 30 rolls (i.e., a small fraction of the cell containing about 2000 rolls) are shown for three values of  $\epsilon$ . At  $\epsilon=0.05$  (two upper figures) defects were never observed. At  $\epsilon=0.1$  (two middle figures) the mean value of defects is about 2. The left figure shows a pair just created. The right figure shows the deformation field of a single defect. The asymmetry of that field indicates that it travels from right to left. The two lower figures show examples at  $\epsilon=0.17$ , where the mean number of defects is about 4.

We have counted the number of defects as a function of time for different values of  $\epsilon$ . Two examples are shown in Fig. 7. The lower curve, measured at  $\epsilon=0.085$ , i.e., very close to the onset of defects, is reminiscent of the intermittent data presented in Fig. 4 of Ref. 5(a). The upper curve ( $\epsilon=0.19$ ), similar to Fig. 1 of Ref. 12, justifies the idea of a statistical description. A theory about the statistics of defects had been presented recently<sup>12</sup> based on the idea that the probability to create a defect pair is given by  $\epsilon$ , while the probability to annihilate a pair is proportional to the density of the defects squared. These mechanisms lead to a squared Poisson distribution:  $P_n = \gamma^n / [I_0(2\gamma^{1/2}) / (n!)^2]$  where  $P_n$  is the probability to have  $n$  pairs of defects.  $I_0$  is the standard modified Bessel function and  $\gamma^{1/2}$  is the mean value of  $n$ .

The histograms (diamonds) based on counting defects in about 400 pictures for different values of  $\epsilon$  are shown in Fig. 8. A total of 800 pictures had been analyzed for  $\epsilon=0.19$  to reduce the statistical errors. The agreement with the theoretical curves (solid lines) is very good.

I. R. and S. R. were supported by Minerva Gesellschaft für die Forschung m.b.H. We thank D. Allais, E.

Moses, I. Procaccia, and P. Coulet for helpful and stimulating suggestions.

(a)Permanent address: Physikalisches Institut, Universität Bayreuth, D-8580 Bayreuth, West Germany.

<sup>1</sup>H. Brand, P. Hohenberg, and V. Steinberg, *Phys. Rev. A* **30**, 2548 (1984), and references therein.

<sup>2</sup>A. C. Newell, *Lectures in Math.* **15**, 157 (1974); C. S. Bretherton and E. A. Spiegel, *Phys. Lett.* **96A**, 152 (1983); H. R. Brand, P. S. Lomdahl, and A. C. Newell, *Physica (Amsterdam)* **23D**, 345 (1986).

<sup>3</sup>V. Steinberg, E. Moses, and J. Fineberg, *Nucl. Phys. (Proc. Suppl.)* **B2**, 109 (1987).

<sup>4</sup>M. Bestehorn, R. Friedrich, and H. Haken (to be published).

<sup>5</sup>(a) P. Coulet, L. Gil, and J. Lega (to be published); (b) P. Coulet and J. Lega (to be published).

<sup>6</sup>For reviews, see W. J. A. Goossens, in *Advances in Liquid Crystals*, edited by G. H. Brown (Academic, New York, 1978); L. M. Blinov, *Electro-Optical and Magneto-Optical Properties of Liquid Crystals* (Wiley, New York, 1983).

<sup>7</sup>S. Rasenat, G. Hartung, B. L. Winkler, and I. Rehberg (to be published).

<sup>8</sup>E. O. Schulz-DuBois and I. Rehberg, *Appl. Phys.* **24**, 323 (1981).

<sup>9</sup>A. Joets and R. Ribotta, *Phys. Rev. Lett.* **60**, 2164 (1988).

<sup>10</sup>E. Moses, J. Fineberg, and V. Steinberg, *Phys. Rev. A* **35**, 2757 (1987); R. Heinrichs, G. Ahlers, and D. S. Cannell, *ibid.* **35**, 2781 (1987); J. Fineberg, E. Moses, and V. Steinberg, *Phys. Rev. Lett.* **61**, 838 (1988); P. Kolodner and C. Surko, *ibid.* **61**, 842 (1988).

<sup>11</sup>P. Coulet, in *Proceedings of the Conference on Advances in Fluid Turbulence*, Los Alamos, May 1988 (unpublished).

<sup>12</sup>L. Gil, J. Lega, and J. L. Meunier (to be published).